

## Growth of order in an anisotropic Swift-Hohenberg model

Hai Qian and Gene F. Mazenko

*The James Franck Institute and Department of Physics, The University of Chicago, Chicago, Illinois 60637, USA*

(Received 24 July 2005; published 14 March 2006)

We have studied the ordering kinetics of a two-dimensional anisotropic Swift-Hohenberg (SH) model numerically. The defect structure for this model is simpler than for the isotropic SH model. One finds only dislocations in the aligned ordering striped system. The motion of these point defects is strongly influenced by the anisotropic nature of the system. We developed accurate numerical methods for following the trajectories of dislocations. This allows us to carry out a detailed statistical analysis of the dynamics of the dislocations. The average speeds for the motion of the dislocations in the two orthogonal directions obey power laws in time with different amplitudes but the same exponents. The position and velocity distribution functions are only weakly anisotropic.

DOI: [10.1103/PhysRevE.73.036117](https://doi.org/10.1103/PhysRevE.73.036117)

PACS number(s): 05.70.Ln, 64.60.Cn, 64.60.My, 64.75.+g

### I. INTRODUCTION

There is ongoing interest in the growth kinetics of stripe-forming systems. There has been progress via experimental [1,2] and numerical [3,4] studies of growth after a quench from an isotropic initial state. However, the theoretical understanding of such systems remains limited. This is mostly due to the complexity of the defect structures generated during ordering in such systems. For example, in the Swift-Hohenberg model, there are grain boundaries, disclinations, and dislocations generated in the ordering process. The coexistence of all these different defect structures has hindered the theoretical analysis of the striped phase-ordering systems. In this paper, we study an anisotropic Swift-Hohenberg (SH) model, where only dislocations are produced in the ordering process. Our goal is to understand the statistical properties of these defects much as we now understand those properties for simple vortex-producing models.

There are formal arguments [5] that if we break the symmetry of the isotropic SH model by applying, for example an electric field, then the system can be mapped onto an isotropic time-dependent Ginzburg-Landau (TDGL) model. This suggests a  $L \approx t^{1/2}$  growth law compared to much slower growth in the isotropic SH model. We find support for this hypothesis.

Some previous studies have focused on the evolution of a few dislocations [6–12]. Tesauro and Cross [6] studied the steady-state climbing motion (move along the direction of stripes) of isolated dislocations both theoretically and numerically in several two-dimensional model systems including the SH model. They found that the wave number selected by the dislocation climb is marginally stable only for potential models. Bodenschatz *et al.* [11] studied the climbing motion of dislocations with amplitude equations appropriate for systems with an axial anisotropy. The Peach-Koehler (PK) force (the effective wave-number mismatch) drives the dislocation motion, just as in Ref. [6]. They also consider the interaction between two dislocations together with the PK force. Goren *et al.* [7–9] studied the convection in a thin layer of a nematic material experimentally. They introduced a gauge-field theoretical treatment to study the climbing of dislocations in a stressed background field where the PK

force plays a role. The theory [12] predicts that climbing and gliding motions of a single dislocation are equivalent (after the proper scaling for the anisotropic system) and due to the PK mechanism. Braun and Steinberg [10] studied the same experimental system. They measured the gliding motion of dislocations due to a pure interaction between the members of the pair without the PK mechanism. They found that the climb and gliding motion have different characters.

Boyer [13] simulated an anisotropic stripe-forming model [14] based on the Swift-Hohenberg model. His model is more complicated than ours. In his model the stripes have two preferred directions and a zigzag pattern is formed, and the dislocations tend to stay together to form large domain walls. The author found that for small quenches the energy, the dislocation energy, and the characteristic length normal to the stripes all scale as  $t^{\pm 1/2}$  (+ for the characteristic length). He also found that for deep quenches the system was frozen. The pinning effect becomes important as the quench depth increases. The zigzag pattern was experimentally realized in Ref. [15].

Here we study an ensemble of well-separated dislocations in the context of domain growth. The motion of the dislocations in this model is highly anisotropic. They tend to move across the stripes. The average speeds across and along the stripes obey simple power laws in time with different amplitudes but approximately the same exponent. The distributions of the defect velocities along the two orthogonal directions have same form and large velocity power-law tails with approximately the same exponents. Two bulk measurements of the ordering—the decay of the effective energy and the number of dislocations—obey a simple power law in time with a logarithmic correction, as for the XY model [18].

The two-dimensional isotropic SH model [19] is defined by a Langevin equation

$$\frac{\partial \psi(\mathbf{x}, t)}{\partial t} = - \frac{\delta \mathcal{H}[\psi]}{\delta \psi(\mathbf{x}, t)} + \xi(\mathbf{x}, t), \quad (1)$$

where  $\psi$  is the ordering field and the effective Hamiltonian is given by

$$\mathcal{H}[\psi] = \int d^2r \left\{ -\frac{\epsilon}{2}\psi^2 + \frac{1}{2}[(\nabla^2 + 1)\psi]^2 + \frac{1}{4}\psi^4 \right\}, \quad (2)$$

where  $\epsilon$  is a positive constant. All the quantities in this paper have been put in dimensionless form. The noise  $\xi$  satisfies  $\langle \xi(\mathbf{x}, t) \xi(\mathbf{x}', t') \rangle = 2T \delta(\mathbf{x} - \mathbf{x}') \delta(t - t')$ , where  $T$  is the temperature after the quench. In the following, we set  $T=0$  which eliminates the noise term from the analysis. Starting from a random initial condition without long-distance correlations, the SH equation (1) generates stripes with period  $2\pi$ .

In the simulations for the isotropic SH model, we found [4] that the grain boundaries' motion dominates the ordering dynamics of the system, which is different from what is seen in some experiments [1,2], where the disclination quadrupole annihilation is the dominant ordering process. Disclinations and dislocations are also present in the SH ordering system. In more recent experiments [16] on different diblock copolymer systems, defect configurations looking more like the SH simulations [4] are found. The coexistence of different kinds of disordering defects makes it difficult to analyze simulations of the isotropic SH system. However, in an anisotropic SH system, where only pointlike dislocations are present, the system should be easier to study.

We make the SH system anisotropic by adding an additional term to the effective Hamiltonian

$$\mathcal{H}[\psi] \rightarrow \mathcal{H}[\psi] + \int d^2r \frac{\gamma}{2} \left( \frac{\partial \psi}{\partial y} \right)^2, \quad (3)$$

where  $\gamma$  is a constant. The anisotropic term corresponds to applying an external magnetic field. In this case the SH equation now takes the form

$$\frac{\partial \psi}{\partial t} = \epsilon \psi + (\nabla^2 + 1) \psi - \psi^3 + \gamma \frac{\partial^2 \psi}{\partial y^2}. \quad (4)$$

We studied the case where  $\epsilon=0.1$  and  $\gamma=0.4$ . Stripes generated by the above equation align along the  $y$  direction on the  $x$ - $y$  plane. This configuration minimizes the anisotropic term in Eq. (3). We start from a random initial condition for  $\psi$ . After a very short transient time, the only defects left in the system are dislocations. Dislocation annihilation is the final ordering process.

In Sec. II, we set up our numerical study. Then in Sec. III we study the time decay of the system energy. The stripe patterns and the motions of the dislocations are shown in Sec. IV. And we analyze the quantitative measurements in Sec. V. The speed distribution for the dislocations is shown in Sec. VI.

## II. NUMERICAL ALGORITHM

We employed the usual Euler method to drive the system:

$$\psi(t + \Delta t) = \psi(t) + \Delta t [\epsilon \psi(t) - (1 + \nabla^2)^2 \psi(t) + \gamma \partial_y^2 \psi(t) - \psi(t)^3]. \quad (5)$$

We take in this case time step  $\Delta t=0.02$  and lattice spacing  $\Delta r=\pi/4$ . In the following sections, the numerical measurements are obtained from the system that is evolved by the Euler method.

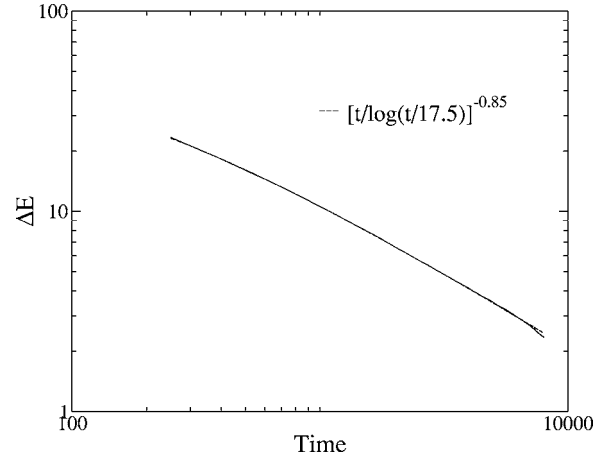


FIG. 1.  $\Delta E$  vs time  $t$  after the quench. The energy  $\Delta E$  is proportional to  $[t/\log(t/18.5)]^{-0.85}$ . All averages are of 528 runs.

## III. TIME DECAY OF THE AVERAGE ENERGY

The first quantity we look at is a gross statistical measure of the ordering given by the average coarse-grained energy  $E = \langle \mathcal{H} \rangle_t$ . In Fig. 1 we plot  $\Delta E = E - E_0$ , where  $E_0$  is the ordered value of  $E$  (known to be accurately given by  $E_0 = -\epsilon^2 S/6$ , where  $S$  is the surface area of the system). These simulations were averaged over 528 runs. In agreement with the  $n=d=2$  TDGL model [17,18] we find a power law with a logarithmic correction characteristic of the annihilation of point defects. This is clearly consistent with a growth-law exponent of  $z \approx 2$ . Although Fig. 1 does not give a good estimate for the exponent  $z$ , we conclude that  $z=2$  is the best value by taking into account Fig. 6 discussed below. Having established that the ordering is speeded up relative to the isotropic SH model, where  $z \approx 3$ , we can move on to look at the nature of the ordering patterns grown using this model.

## IV. DISLOCATIONS

In Fig. 2 we show a typical ordering configurations of the anisotropic SH system at different times. Notice that the only defects produced are dislocations.

We are interested in the path of each dislocation trajectory. These paths must be determined accurately enough such that we can compute dislocation speeds. In the case of the  $O(2)$  TDGL model [17,18] we were able to accurately determine the position of a vortex by finding the zeros (minima) in the order parameter amplitude. Here the situation is more complicated. As explained in Ref. [4] the positions of defects in the SH model are located by maxima in the quantity

$$A = \sum_{\alpha} (\nabla_{\alpha} \phi)^2, \quad (6)$$

where  $\phi$  is the angle that the director  $\hat{n} = \nabla \psi / |\nabla \psi|$  makes with some arbitrary direction and  $\alpha$  is the index for different spatial directions. We showed numerically that if  $A > A_0$ , then that site on the lattice can be associated with a defect. Here we need to determine the position of the dislocation with some accuracy. We have found that the expression

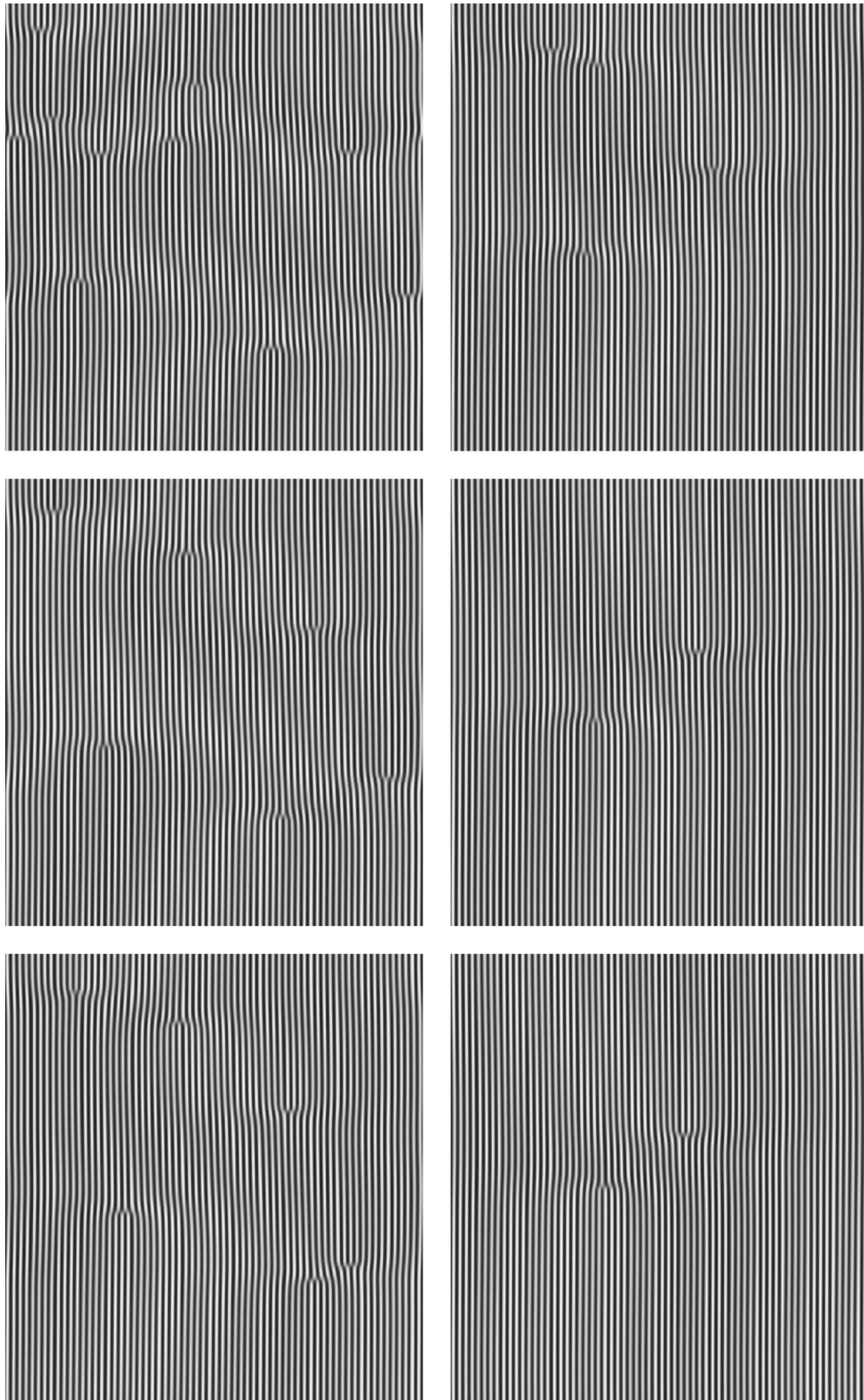


FIG. 2. Typical configurations of an  $512 \times 512$  anisotropic SH system at different times. From left to right and top to bottom, the system was at  $t=2500$ ,  $5000$ ,  $7500$ ,  $10\,000$ ,  $12\,500$ , and  $15\,000$ .

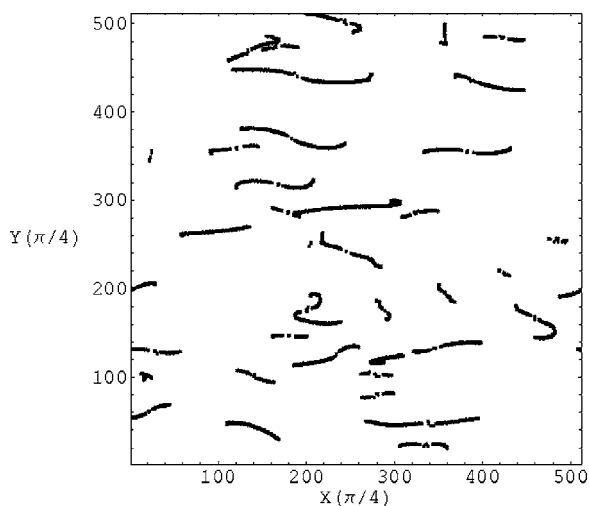


FIG. 3. The trajectories of the dislocations in a  $512 \times 512$  anisotropic SH system. The dots are the positions where two dislocations annihilate. The stripes are along the  $y$  direction as shown in Fig. 2. Most of the dislocations glide across the stripes.

$$\bar{r}_\alpha = \frac{\sum_i r_\alpha^i A_i}{\sum_i A_i} \quad (7)$$

gives the position of the dislocation in the  $\alpha$ th direction, and the sum is over all contiguous sites where  $A_i > A_0 = 3.0$ . Using these procedures we obtain, for example, the set of dislocation trajectories shown in Fig. 3. The dislocations tend to move (glide) across the stripes and annihilate with each other. If we look more closely we see the oscillating behavior in the glide motion as shown in Figs. 4 and 5. In Fig. 4 we also show all the sites that are associated with the dislocations. To obtain useful statistical data we will need to average over the different runs for our system.

The oscillation in the glide motion of the dislocation is due to Peierls-like pinning forces. The law of motion of a

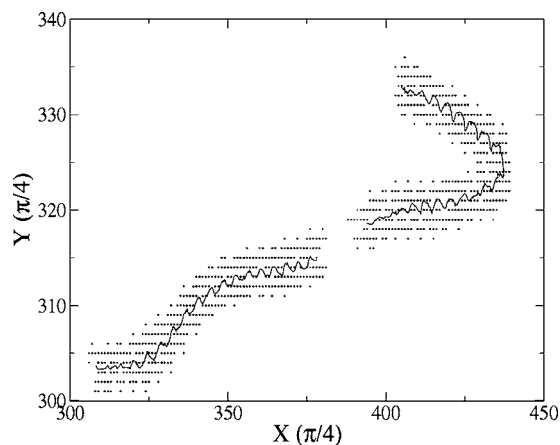


FIG. 4. The trajectories of two annihilating dislocations. The solid line denotes the center of the dislocation core determined by Eq. (7). The dots indicate the sites  $i$  which are part of the core used in Eq. (7). Thus this figure shows the motion of the dislocation core.

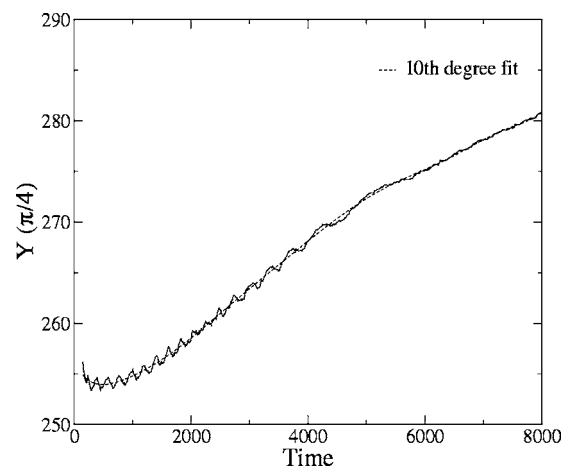


FIG. 5. The position of a dislocation along the stripes versus the time after the quench. We use a tenth-degree polynomial to fit the data and average out the oscillations along the  $y$  direction.

dislocation due to the Peierls-like force takes the form [13]

$$\mu^{-1}v = \mu^{-1} \frac{dx}{dt} = f - p \cos(kx).$$

Here  $v$  is the velocity across the stripes.  $\mu$  is the mobility.  $f$  is the external force per unit length applied onto the dislocation. In this context,  $f$  is caused by other dislocations, especially the one that is going to annihilate with the dislocation of interest.  $p$  is the magnitude of the pinning force. The Peierls-like pinning force term oscillates with a period of  $2\pi/k$ , which is exactly the stripe pattern period. We are interested in the interaction  $f$  between dislocations. In the next section, we will compute the average  $v$  versus the separation distance between two annihilating dislocations.

We plot the average number of dislocations,  $N_d$ , as a function of time in Fig. 6. Clearly it is fit by a power law with a logarithmic correction just as for  $\Delta E$  and the isotropic TDGL result for  $n=d=2$  [17,18].  $N_d$  and  $\Delta E$  share approximately the same time dependence with growth-law exponent  $z \approx 2$ .

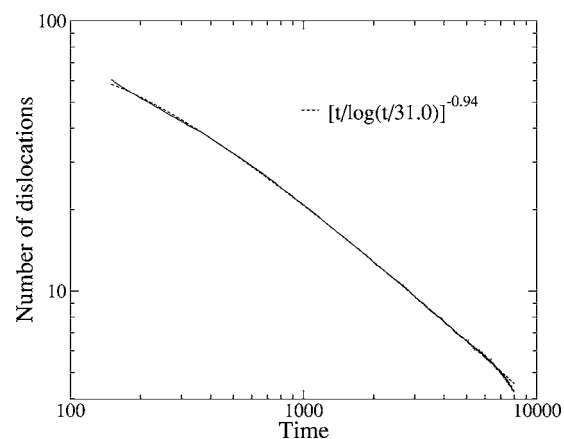


FIG. 6. The number of dislocations,  $N_d$ , for the anisotropic SH model as a function of time averaged over 528 runs is given by the solid line. There is an excellent fit to the form  $[t/\log(t/a)]^{-b}$  with  $a=32.1$  and  $b=0.94$ .

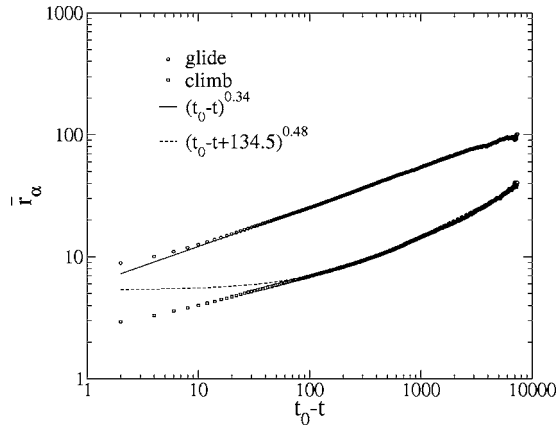


FIG. 7. The average distance between two dislocations which are going to annihilate with each other versus time before the annihilation. The components across (glide) and along (climb) the stripes are measured, respectively.

The energy per dislocation is almost a constant, which means the dislocations control the dynamics of the system.

### V. ANALYSIS

To quantify the extent of cross stripe migration of dislocations, we measured the average distance  $r_\alpha$  in the climb and glide directions between two dislocations which are going to annihilate with each other at time  $t_0$ . In Fig. 7, we show  $r_\alpha$  vs  $t-t_0$ , where  $t$  is the time we measure the distance. We measured the components of average distance across and along the stripes. In Fig. 7, we can see that at any  $t-t_0$  the separation of two annihilating dislocations across the stripes is much larger than the distance along the stripes. This means the two dislocations tend to approach each other along the direction across the stripes. We notice that the average separation takes a power-law form for the glide motion. The climbing motion as one approaches annihilation is more complicated.

If we plot the average separation of defects heading toward annihilations versus time after quench we obtain the result shown in Fig. 8. Unlike in the NCOP TDGL case  $\bar{r}$  deviates from a power-law behavior for long times and does not serve as a good measure of the growth law for the system.

In Ref. [17] we found good scaling results and a reasonable theoretical model for describing the numerical results because there was a simple scaling relation between the average separation  $r$  of two annihilating defects and their relative speed  $u$ ,  $u \sim r^{-b}$ . The situation is more complicated here. In Fig. 9 we plot the average relative speed in a given direction versus separation in that direction. As the dislocations approach each other, their speeds increase. And when the distance between them is too small, our measurement is unable to follow the motions of the dislocations. So the data points in Fig. 9 with distances smaller than  $r=16$  are not reliable and should not be taken into account in the following analysis.

Using only the reliable data in Fig. 9 we obtain

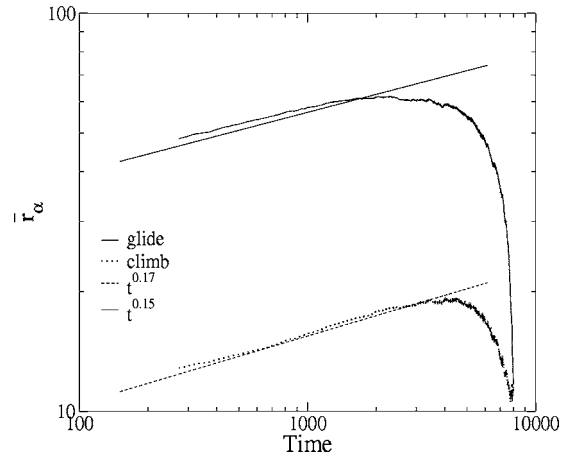


FIG. 8. The average distance between two dislocations which are going to annihilate versus the time after the quench. The components across (glide) and along (climb) the stripes are measured respectively.

$$u_\alpha = A_\alpha r_\alpha^{-b}, \quad (8)$$

where  $b=0.75$  for both climb and glide and  $A_g=0.58$  and  $A_c=0.06$ . The assumption  $\bar{u}_\alpha = \bar{u}_\alpha(r_\alpha)$  is only approximately correct. In fact  $\bar{u}_\alpha$  depends on both  $x$ -separation and  $y$ -separation distances, as is shown in Fig. 10(a). Correspondingly, there is a strong correlation as shown in Fig. 10(b) between the glide separation  $d_g$  and the separation distance  $d$ . The climb distance is correlated with  $d$  for small enough separations.

If we plot the average relative speed versus time to annihilation, Fig. 11, we obtain the approximate power-law result

$$\bar{u}_\alpha(t) \sim (t_0 - t)^{-1/z}, \quad (9)$$

which is consistent with  $z=2$  in both directions.

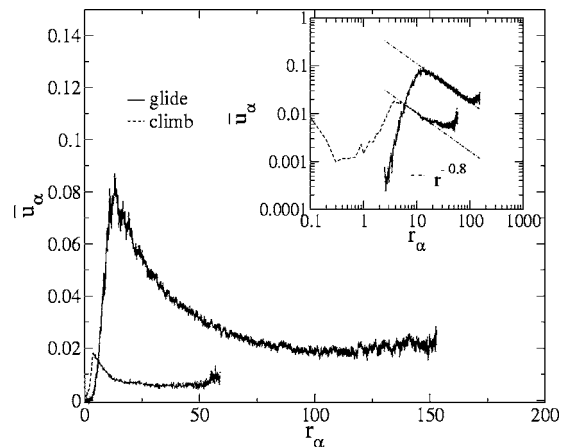


FIG. 9. The average relative speed between two dislocations which are going to annihilate versus the separation between them in that direction. The best fit for each set of the glide data is given by  $u(r_\alpha) = A_\alpha r_\alpha^{-b}$  with  $b_\alpha = 0.75$  approximately for both glide and climb.

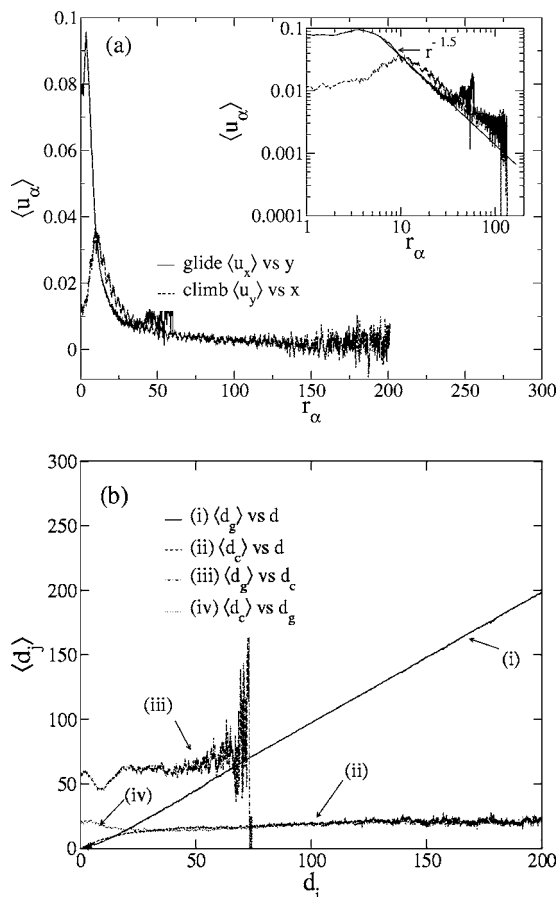


FIG. 10. (a) The speed  $u_x$  and  $u_y$  depend on both  $x$  and  $y$ . (b)  $d$  is the distance between two annihilating dislocations.  $d_g$  is the separation distance across the stripes (glide motion).  $d_c$  is the separation distance along the stripes (climb motion). And  $d^2 = d_c^2 + d_g^2$ .

VI. PROBABILITY DISTRIBUTIONS

We can next turn to the associated probability distributions. The first is the separation probability distribution. This is the probability  $P_r^\alpha(t)$  that at time  $t$  two annihilating dislocations are separated by a distance  $r_\alpha$ , where  $\alpha$  corresponds to climb or glide. We assume that  $P_r^\alpha(t)$  takes a scaling form if we plot it versus  $r_\alpha/\bar{r}_\alpha(t)$  as shown in Fig. 12, where the average  $\bar{r}_\alpha$  is shown in Fig. 8. We obtain a reasonable scaling form but unlike in Ref. [17] we do not find an algebraic large separation tail. Instead the scaling function appears to decay exponentially. Notice that the scaling forms are roughly independent of direction. We fit the separation distribution function with  $y = a_0 x^b / (1 + a_1 x^{1+b})^c$ , where  $a_0$ ,  $a_1$ ,  $b$ , and  $c$  are parameters. This function is the most general form for the separation distribution obtained from [17]. Since the fitting function has a power-law decay tail, which is different from the exponential decay of the real data, we are unable to fit the large separation tail. When we fit the data, we restrict the value of  $c$  to be between 1 and 5. The resulting value of  $c$  is 4.9. If we extend the upper limit on  $c$ , the best fit for  $c$  increases. However, we found that  $b$  is always close to 0.7 whatever the upper limit of  $c$ .

We turn next to the statistics governing the relative speeds. The average speeds are shown in Fig. 13(a) to be

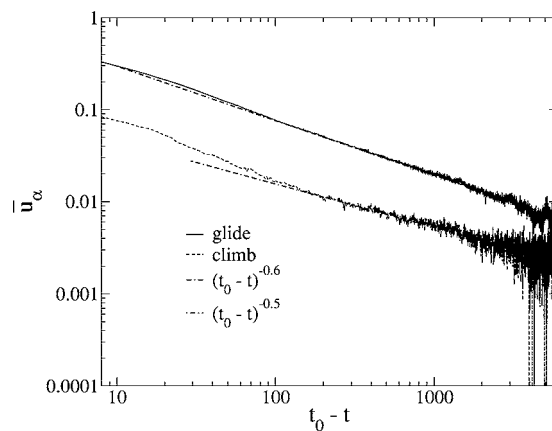


FIG. 11. The average relative speed between two dislocations which are going to annihilate versus the time before the annihilation in the glide and climb directions.

given approximately by  $t^{-1/2}$  for both directions in agreement with the scaling ideas. If we fit the climb trajectories in a way that averages over the oscillations in the climb component, we obtain the average climb speed which is in better agreement with the  $t^{-1/2}$  result, as is shown in Fig. 13(b).

Finally we plot the speed distribution function in Fig. 14(a). Clearly we have a large speed power-law tail. We find roughly that both glide and climb motions have a  $v^{-3}$  large speed power-law tail as shown in Fig. 14(b) after we average out the oscillations on the  $y$  component (along the stripes). The distribution functions are sensitive to how we treat the oscillations in the climb data. This may account for the higher tail exponent 3.9 shown in Fig. 14(a) for the climb data. We also use a quite general form for the speed distribution function obtained from Ref. [17] to fit the data. The function is  $y(x) = a_0 x^{-2 + [c(b+1) - 1]/b} / (1 + a_1 x^{(b+1)/b})^c$ . We require that  $y(0)$  to be nonzero. So we must have  $-2 + [c(b+1) - 1]/b = 0$ . The parameter  $b$  is the same  $b$  in Fig. 9, with a value 0.8. So we have  $c = (1 + 2b)/(1 + b) = 1.44$ . So we fix the

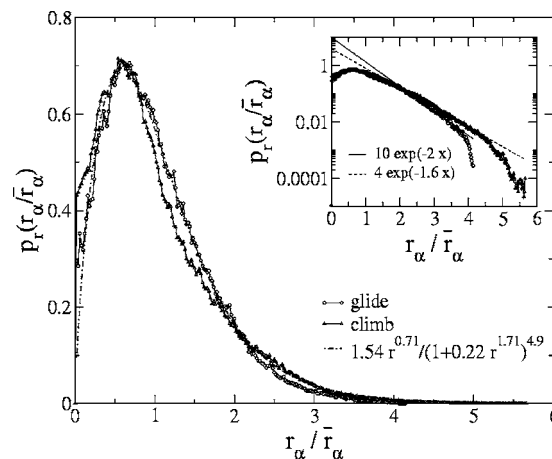


FIG. 12. The separation probability distribution. The tail of the distribution has an exponential form, as is shown in the inset. We fit the separation distribution function with  $y = a_0 x^b / (1 + a_1 x^{1+b})^c$ , where  $a_0$ ,  $a_1$ ,  $b$ , and  $c$  are parameters whose values are given in the figure.

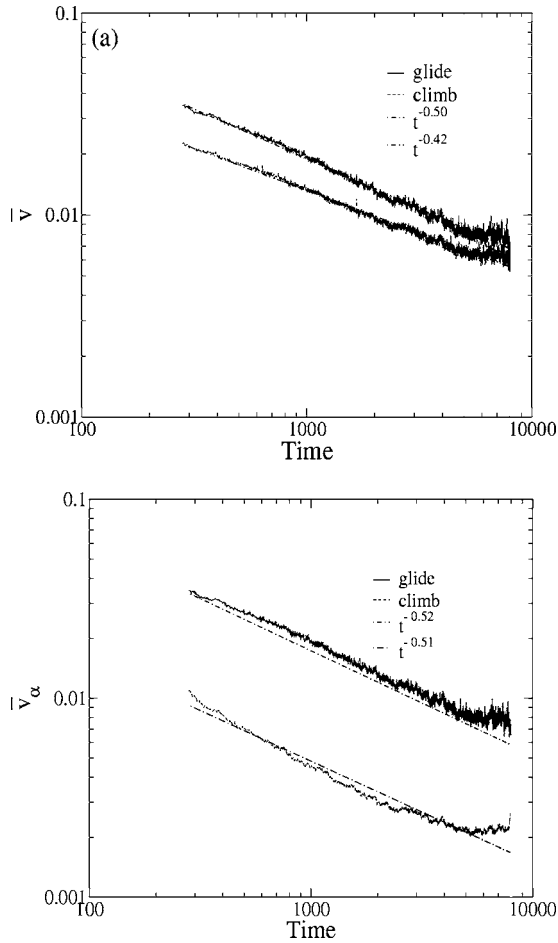


FIG. 13. (a) The averages of the speeds, the transverse component (across the stripes), and the longitudinal component (along the stripes). They all obey simple power laws  $\bar{v}_\alpha \sim t^{x_\alpha}$ . In (b), we use a tenth-degree polynomial to fit the trajectories of climb motion and average out the oscillations on climb motion. The obtained power-law exponent is closer to 0.5 in this case.

values of  $c=1.44$  and  $b=0.8$  in the curve fitting.

Again the scaling forms in the two directions are, to within our accuracy, equivalent.

## VII. CONCLUSION

The kinetics of the anisotropic SH model are conceptually simpler than for the isotropic SH case since there is only one disordering defect. In the simplest picture one has a set of point defects ordering in a fashion similar to a collection of vortices in an XY model [18] but with anisotropic scaling. One has a scaling length  $L_\alpha(t) \sim A_\alpha t^x$  and power-law behaviors for the decreasing energy, number of defects, and average defect velocity with  $x \sim 0.5$ .

The picture of annihilating point defects with a growth law of  $t^{1/2}$  is roughly true for our anisotropic system, and in this sense the system is similar to the two-dimensional XY model with the annihilation of vortices. Both have bulk properties  $\Delta E$  and  $N_d$  which have the same ordering time dependence. Both systems have large velocity power-law tails which show  $v^{-3}$  behavior. One simple result is that the scal-

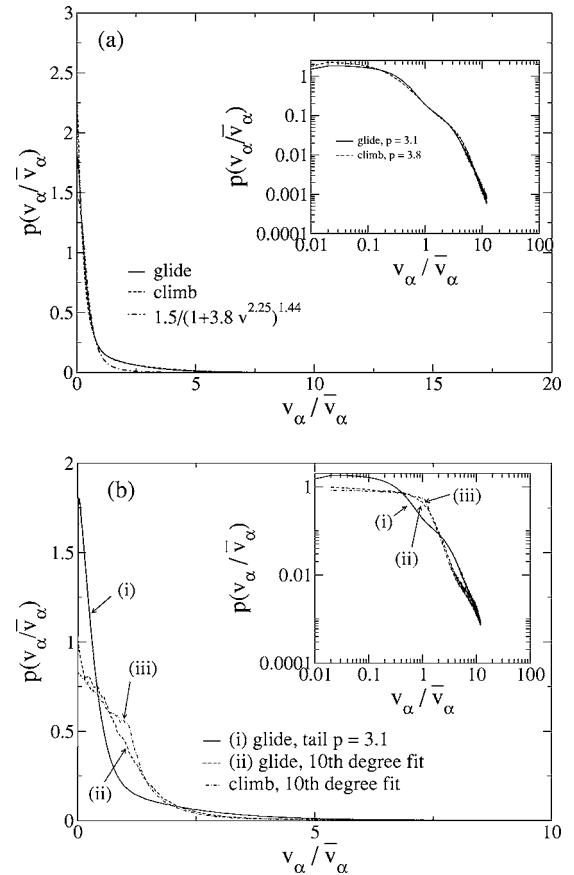


FIG. 14. The distribution of the defects' speed for glide and climb directions. After scaling the data at different times (from 300 to 8000), we collapse all the speed data to one curve. The motions of gliding and climbing are measured separately. In (b), the oscillations of the climbing motion along the stripe are averaged out. We also use a tenth-degree polynomial to smooth the glide motion.

ing functions  $P(r)$  and  $P(v)$  are nearly isotropic as shown in Figs. 12 and 14. This is true despite the fact that the motion is highly anisotropic. It appears that the annihilating defects organize themselves in such a way that their relative velocity is radial. Once this is true, it is not important what the angle is between the relative velocity and the stripes. As one looks closer the analogy breaks down. The separation probability distribution shows a clear power-law tail in the XY model but not in the anisotropic model. The average distance between annihilation defects in the XY model serves as a good measure of the growth law  $\bar{r} \sim t^{1/2}$ . This is not true in the anisotropic model where  $\bar{r} \sim t^{0.17}$ . One interpretation of our results is that the hypothesis of independent pairs of dislocations breaks down at a much greater distance than for the XY model. It is also possible that the independent pair mechanism used in Ref. [17] works less well in this system. There may be correlations among different pairs of dislocations. In any event, our results cannot be simply explained by a rescaling of the glide and climb directions.

## ACKNOWLEDGMENT

This work is supported by the Material Science and Engineering Center through Grant No. NSF DMR-9808595.

- [1] C. Harrison, D. H. Adamson, Z. Cheng, J. M. Sebastian, S. Sethuraman, D. A. Huse, R. A. Register, and P. M. Chaikin, *Science* **290**, 1558 (2000).
- [2] C. Harrison, Z. Cheng, S. Sethuraman, D. A. Huse, P. M. Chaikin, D. A. Vega, J. M. Sebastian, R. A. Register, and D. H. Adamson, *Phys. Rev. E* **66**, 011706 (2002).
- [3] J. J. Christensen and A. J. Bray, *Phys. Rev. E* **58**, 5364 (1998).
- [4] H. Qian and G. F. Mazenko, *Phys. Rev. E* **67**, 036102 (2003), and references therein.
- [5] L. M. Pismen, *Vortices in Nonlinear Fields* (Oxford University Press, London, 1999), p. 63.
- [6] G. Tesauro and M. C. Cross, *Phys. Rev. A* **34**, 1363 (1986).
- [7] G. Goren, I. Procaccia, S. Rasenat, and V. Steinberg, *Phys. Rev. Lett.* **63**, 1237 (1989).
- [8] S. Rasenat, V. Steinberg, and I. Rehberg, *Phys. Rev. A* **42**, 5998 (1990).
- [9] L. Kramer, E. Bodenschatz, and W. Pesch, *Phys. Rev. Lett.* **64**, 2588 (1990).
- [10] E. Braun and V. Steinberg, *Europhys. Lett.* **15**, 167 (1991).
- [11] E. Bodenschatz, W. Pesch, and L. Kramer, *Physica D* **32**, 135 (1988).
- [12] E. Bodenschatz, W. Pesch, and L. Kramer, *Physica D* **32**, 5 (1988).
- [13] D. Boyer, *Phys. Rev. E* **69**, 066111 (2004).
- [14] W. Pesch and L. Kramer, *Z. Phys. B: Condens. Matter* **63**, 121 (1986).
- [15] C. Kamaga, F. Ibrahim, and M. Dennin, *Phys. Rev. E* **69**, 066213 (2004).
- [16] W. Lopes (private communication).
- [17] H. Qian and G. F. Mazenko, *Phys. Rev. E* **70**, 031104 (2004).
- [18] H. Qian and G. F. Mazenko, *Phys. Rev. E* **68**, 021109 (2003).
- [19] J. Swift and P. C. Hohenberg, *Phys. Rev. A* **15**, 319 (1977).